

DYNAMIC SIMULATION OF SMALL SOLAR SYSTEM BODIES

S. L. SEMENOVA¹ and V. M. CHEPUROVA²

¹*Institute of Science and Technique Information of Russian Academy of Science,
Astron. Depart., ul. Usievicha 20A, 125219 Moscow, Russia*

²*Sternberg State Institute of Astronomy, Celest. Mech. Depart., Universitetskii
pr. 13, 119899 Moscow, Russia*

(Received June 20, 1996)

As part of a dynamical study of small transneptunian bodies, in particular, of the cometary Oort cloud, a simulation of orbital evolution under the influence of the Galactic gravitational field was performed. The tidal Galactic potential includes a term corresponding to the Sun's orbital motion around the Galaxy's centre (core) in the point-mass approximation, when the point-mass Galactic core has the total mass of the Galaxy.

KEY WORDS Comets, Oort cloud, tidal Galactic potential, Sun's orbital inclination, dynamic simulation

The first part of the simulation is the comparison of two analytical forms for the Galactic potential, presented by P. P. Parenago (1950a, 1950b) and by A. Brunini (1993), but taking into account the Sun's orbital motion, resulting in the modified restricted three-body problem.

We used (as in our papers (1987, 1988, 1989)) the rectangular coordinate system *OXYZ* with origin located at the Sun and (*XY*)-plane coinciding with the mean Galactic disc plane (the *OZ*-axis is in the direction of the Galactic pole). Then the equations of particle motion are given by:

$$\begin{aligned}\frac{d^2x}{dt^2} + \frac{fmx}{r^3} &= \frac{\partial U}{\partial x} + R_x, \\ \frac{d^2y}{dt^2} + \frac{fmy}{r^3} &= \frac{\partial U}{\partial y} + R_y, \\ \frac{d^2z}{dt^2} + \frac{fmz}{r^3} &= \frac{\partial U}{\partial z} + R_z,\end{aligned}\tag{1}$$

where $r^2 = x^2 + y^2 + z^2$ is the radius-vector of the particle, f is the gravitational constant, m is the total mass of the Sun, M_\odot , and the outer planets, $R_{x,y,z}$ are the components of the disturbing function, including the orbital motion of the Galactic

core around the Sun (in the given frame of reference), and

$$U_{\text{Par}} = \frac{\Phi_c \exp(-\lambda z^2)}{(1 + \kappa \Delta)}, \quad (2)$$

$$U_{\text{Br}} = 2\pi f \rho z^2, \quad (3)$$

assuming that Φ_c is the gravitational potential at the Galactic centre, $\vec{\Delta} = \vec{R} - \vec{r}$, and R is a constant, the radius of the Sun's circular (that is, Galactic core) orbit. In other words, $\vec{\Delta}$ is the distance between the particle and the Galactic core. κ and λ are constants and ρ is the mean density in the solar neighbourhood: $\rho = 0.185 \pm 0.02 M_\odot \text{ pc}^{-3}$.

It is obvious that $r/R \ll 1$. Using this ratio as a small parameter it is possible to expand the right-hand sides of the differential equations up to first-order terms. The linearized equations of particle motion for $r/R \ll 1$ are (following Parenago) (I):

$$\begin{aligned} \frac{d^2 x}{dt^2} &= -\frac{fmx}{r^3} - \frac{\Phi_c \kappa}{(1 + \kappa \Delta)^2} \frac{(x - R \cos \omega t)}{\Delta}, \\ \frac{d^2 y}{dt^2} &= -\frac{fmy}{r^3} - \frac{\Phi_c \kappa}{(1 + \kappa \Delta)^2} \frac{(y - R \sin \omega t)}{\Delta}, \\ \frac{d^2 z}{dt^2} &= -\frac{fmz}{r^3} - \frac{\Phi_c \kappa}{(1 + \kappa \Delta)^2} \frac{z}{\Delta} - \frac{2\Phi_c \lambda z}{(1 + \kappa \Delta)}, \end{aligned} \quad (4)$$

and for Brunini's case (II):

$$\begin{aligned} \frac{d^2 x}{dt^2} &= -\frac{fmx}{r^3} + fM_g \frac{x(3 \cos^2 \omega t - 1) + 1.5y \sin 2\omega t}{R^3}, \\ \frac{d^2 y}{dt^2} &= -\frac{fmy}{r^3} + fM_g \frac{y(3 \sin^2 \omega t - 1) + 1.5x \sin 2\omega t}{R^3}, \\ \frac{d^2 z}{dt^2} &= -\frac{fmz}{r^3} + \frac{fM_g z}{R^3} + 4\pi f \rho z, \end{aligned} \quad (5)$$

where ω is the angular velocity of the Galactic core and M_g is the mass of the Galaxy: $M_g = 4 \times 10^{11} M_\odot$. The distance Δ is given by:

$$\Delta = R \left(1 - 2x \frac{\cos \omega t}{R} - 2y \frac{\sin \omega t}{R} + \frac{r^2}{R^2} \right)^{1/2} \quad (6)$$

In this simulation we did not take into account the inclination of the Sun's orbit to the mean Galactic disc plane. Both systems (I) and (II) were numerically integrated by the Everhart integrator, written in FORTRAN (subroutine RADA27) with double precision on an IBM PC AT 386. The right-hand sides of the differential equations were computed with an accuracy of 10^{-13} . Transformations from rectangular coordinates to orbital elements and vice versa were performed by standard subroutines.

As a result we compared, for Parenago's and Brunini's potential expressions, the change (the difference between the final and initial values) in the particle's orbital elements:

$$\begin{aligned}\Delta E_i &= E_i^{\text{fin}} - E_i^{\text{ini}}, \quad i = 1, \dots, 7, \\ \vec{E} &= (n, e, i, M, \omega, \Omega, a).\end{aligned}$$

The total range of initial conditions was divided into several regions, according to the boundaries of the "sphere of action", the sphere of influence and Hill's region for the Sun-Galaxy-particle system.

Taking R as 8.5 kpc we have

$$\begin{aligned}s_1 &= (m/M_g)^{2/5} R = 3.657 \times 10^4 \text{ a.u. (Tisserand)}, \\ s_2 &= 0.5(0.5mM_g)^{1/3} = 8.695 \times 10^4 \text{ a.u. (Opik)}, \\ s_3 &= 1.7 \times 10^5 \text{ a.u. (Hill)}.\end{aligned}$$

There is, however, a certain discrepancy between the estimate of the radius of the solar "sphere of influence"; from 8.695×10^4 to 1.39×10^5 a.u. This should be taken into account when choosing the initial conditions. The value of s_1 is deduced from the equality of the accelerations acting on the particle, and s_2 is found from the equality of the acting forces.

Then the initial conditions for the inner range of the Oort cloud are:

$$\begin{aligned}3.657 \times 10^4 &< a < 8.695 \times 10^4 \text{ a.u.}, \\ e &\in (0.08-0.2) \text{ and } e \in (0.8-0.9)\end{aligned}$$

(for this region the particle orbital periods T_2 are estimated to be $(6-10) \times 10^6$ yr) and for the outer one:

$$\begin{aligned}8.695 \times 10^4 &< a < 1.7 \times 10^5 \text{ a.u.}, \\ e &\in (0.1-0.2) \text{ and } e \in (0.8-0.9).\end{aligned}$$

Our calculations were performed in following system of units: unit of mass - M_\odot ; length unit - 10^4 a.u.; time unit - 10^6 yr. In a given frame of reference $\kappa = 7.23824 \times 10^{-6}$ (length unit) $^{-1}$, $\Phi_c = 5.02832 \times 10^4$ (length unit/time unit) 2 , $\lambda = 1.31625 \times 10^{-10}$ (time unit) $^{-2}$, $\omega = 2.55 \times 10^{-2}$ (time unit) $^{-1}$. The Sun's orbital period is known to be 2.45748×10^2 time units.

In both of the cases we considered we found a number of interesting orbits with $i \sim 0$ (near the Galactic disc plane) and $i \sim 90^\circ$ (perpendicular to it). The qualitative picture of the long-term evolution of the inner region of the Oort cloud at small values of i_{orig} in both simulations is similar. The amplitude of oscillations in Δi is absolutely insignificant ($< 1^\circ$).

Changes in the semimajor axis clearly reveal oscillations with a period of T_2 ; however, in this region

$$\Delta a_{\text{meanBr}} > 0, \quad \Delta a_{\text{meanP}} < 0,$$

that is, Brunini's term leads to a broadening, on average, of the inner region of the Oort cloud with respect to the original orbital elements, and Parenago's term compresses these orbits. In the last case the amplitude of oscillations is greater.

For the orbital eccentricity, Parenago's term clearly showed oscillations with a period of $2T_2$, and Brunini's term gave a period of T_2 , but in the last case the amplitude of oscillations is smaller. Indeed, the stable plane orbits become, on average, more and more elongated.

The orbits in the distant region with $i_{\text{orig}} \sim 90^\circ$ and $10^5 < a_{\text{orig}} < 1.39 \times 10^5$ a.u. show practically the same behaviour for both analytic expressions for the potential: after one orbital period ($\sim 10^6$ yr) they become hyperbolic with continuously increasing values of Δe , and the changes in the semimajor axis and inclination can be approximated by a hyperbola. In all simulations $\Delta i \sim 0$, that is, the orbital plane has a tendency to lie near the Galactic disc.

The angular elements ω and Ω for both simulations exhibit the same secular and long-periodic behaviour. The mean anomaly M is characterized by purely secular behaviour. In our simulations the precession of the nodes and apsides is shown to occur in opposite directions. Indeed, the outer region of the Oort cloud under both forms of tidal potential can be considered as a hyperbolic comet flow from the solar system to the Galaxy (see Tsitsin *et al.* 1984, 1985a, 1985b).

Brunini's form of potential is shown to flatten and to encircle, on average, the non-planar particle orbits; for Parenago's expression, these orbits become more elongated. Numerous escapes of particles from the solar system (when the cometary orbits tend to become hyperbolic) take place at distances of order s_2 .

The typical behaviour of the evolution of the particle orbits in the inner and outer parts is presented on Figures 1 and 2, respectively.

The second dynamical simulation was an attempt to evaluate the influence of the Sun's orbital inclination (to the mean Galactic disc plane) using Brunini's potential. The equations of particle motion, assuming that the Sun's (that is, the Galactic core's) inclination equals θ , are given by:

$$\begin{aligned} \frac{d^2x}{dt^2} + \frac{fmx}{r^3} &= fM_g \frac{x(3 \cos^2 \omega t - 1)}{R^3} \\ &+ fM_g \frac{3 \sin \omega t \cos \omega t (y \cos \theta + z \sin \theta)}{R^3}, \\ \frac{d^2y}{dt^2} + \frac{fmy}{r^3} &= fM_g \frac{y(3 \sin^2 \omega t \cos^2 \theta - 1)}{R^3} \\ &+ fM_g \frac{3 \sin \omega t \cos \theta (x \cos \omega t + z \sin \omega t \sin \theta)}{R^3}, \\ \frac{d^2z}{dt^2} + \frac{fmz}{r^3} &= fM_g \frac{z(3 \sin^2 \omega t \sin^2 \theta - 1)}{R^3} \\ &+ fM_g \frac{3 \sin \omega t \sin \theta (x \cos \omega t + y \sin \omega t \cos \theta)}{R^3} + 4\pi f p z, \quad (7) \end{aligned}$$

when we take into account the first-order terms relative to r/R .

The total Galactic mass located in its core (centre) and moves in a circular orbit (as assumed in the first simulation).

Numerical simulations, using subroutine RADA27 with double precision, were performed for two values of θ : (1) $\theta = 0$ and (2) $\theta = 3.5^\circ$. As a result we compared

Table 1.

t	$\delta n \times 10^3$	t	$\delta n \times 10^3$
3.495826	-0.762939	90.891478	-1.275539
6.991652	-0.846386	94.387305	-0.762939
10.487478	-0.739098	97.883131	0.17881
13.983304	-0.882149	101.378957	-0.655651
17.479130	-0.715256	104.874783	-0.780821
20.974957	-0.905991	108.370609	-0.542402
24.470783	-0.685453	111.866435	-1.364946
27.966609	-0.888109	115.362261	-0.464916
31.462435	-0.691414	118.858087	-1.502037
34.958261	-0.780821	122.353913	-0.441074
38.454087	-0.721216	125.849739	-1.364946
41.949913	-0.649691	129.345566	-0.488758
45.445739	-0.774860	132.841392	-0.971556
48.941565	-0.572205	136.337218	-0.619888
52.437391	-0.852346	139.833044	-0.458956
55.933218	-0.536442	143.328870	-0.840425
59.429044	-0.929832	146.824696	0.149012
62.924870	-0.977516	150.320522	-1.120567
66.420696	-1.001358	153.816348	-0.780821
69.916522	-0.858307	157.312174	-1.406670
73.412348	-1.019239	160.808000	1.245737
76.908174	-0.965595	164.303826	-1.633167
80.404000	-0.959635	167.799653	1.537800
83.899826	-1.072884	171.295479	-1.716614
87.395652	-0.888109	174.791305	1.549721

the corresponding difference in the changes of the orbital elements:

$$\delta E = \Delta E_{(2)} - \Delta E_{(1)},$$

$$E = (n, e, i, M, \omega, \Omega, a).$$

The integration interval included one solar orbital period T_1 . Figures 1 and 2 show oscillations of the orbital elements of very small amplitude with an obvious period of $1/2T_1$. The order of magnitude for the difference in changes of the orbital elements is:

$$\delta n \sim 2 \times 10^{-5}, \quad \delta i \sim (1 - 3.1^\circ),$$

$$\delta \omega \sim (1 - 3^\circ), \quad \delta \Omega \sim (1 - 2^\circ),$$

$$\delta a \sim 10^3 \text{ a.u.}$$

Short-period oscillations have periods comparable to the particle orbital period T_2 . In short-term behaviour the largest difference of the orbital elements occurred at $2T_2$. Table 1 demonstrates the order of magnitude for the oscillations in the orbital elements (in particular δn) with respect to θ .

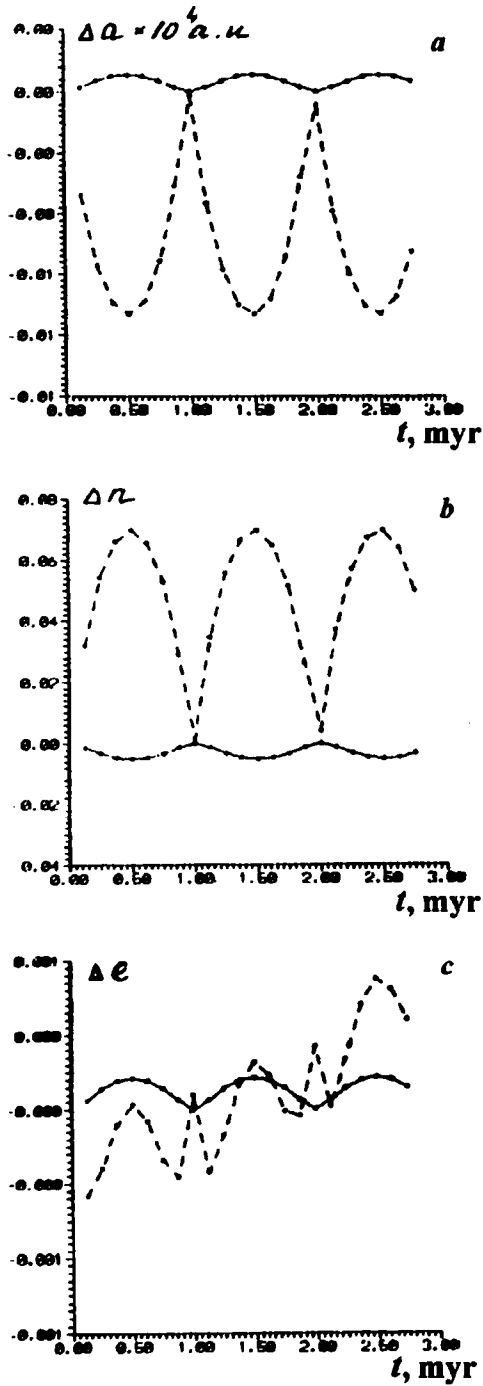


Figure 1 The orbital evolution of the inner part of the Oort cloud (for a , n and e).

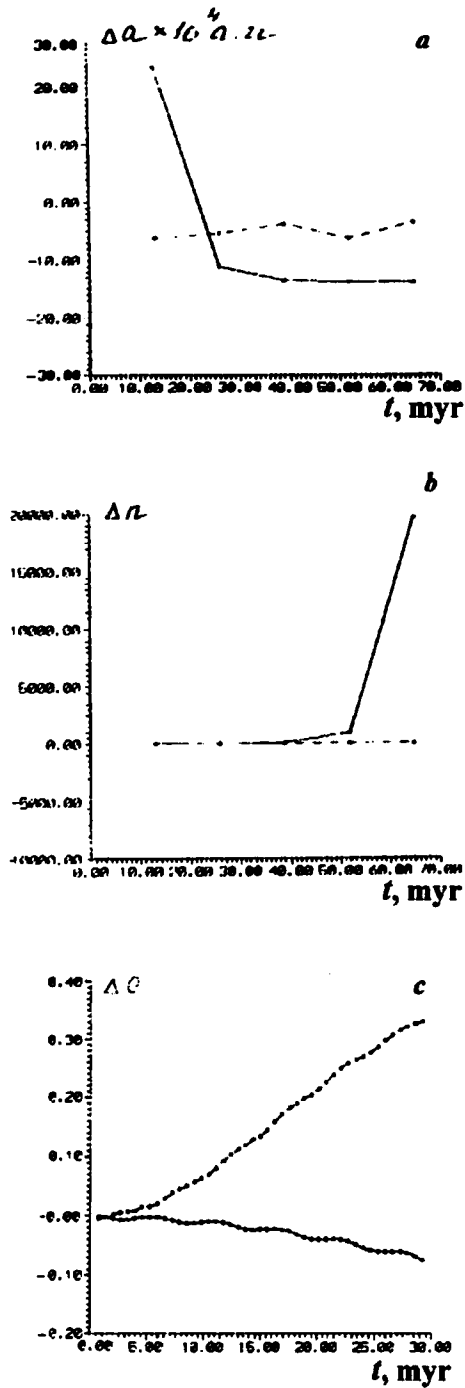


Figure 2 The orbital evolution of the outer part of the Oort cloud (for a , n and e).

We concluded that the component of dynamical friction induced by the non-planar solar orbital motion has a negligible effect on the dynamics of the Oort cloud, contrary to Brunini's note (1993).

References

- Brunini, A. (1993) *Astron. Astrophys.* **273**, 684–694.
Chepurova, V. M. and Shershkina (Semenova), S. L. (1987) *Astron. Chirk.*, No. 1478, 5.
Chepurova, V. M., Kirushenkova, N. V., Shershkina (Semenova), S. L. (1988) *The Analysis of Celestial Body Motions and the Estimation of the Accuracy of their Observations*, Riga, 72–92.
Chepurova, V. M., Shershkina (Semenova), S. L. (1989) *Thes. rep. Conf., Methods of Studying the Motion, Physics and Dynamics of Small Solar System Bodies*, Dushanbe, p. 70.
Parenago, P. P. (1950a) *Astron. J.* **27**, 329.
Parenago, P. P. (1950b) *Astron. J.* **29**, 245.
Tsitsin, F. A., Chepurova, V. M., and Rastorguev, A. S. (1984) *Astron. Chirk.*, No. 1310, 5–6.
Tsitsin, F. A., Chepurova, V. M., and Rastorguev, A. S. (1985a) *Astron. Chirk.*, No. 1378, 1–4.
Tsitsin, F. A., Chepurova, V. M., and Rastorguev, A. S. (1985b) *Astron. Chirk.*, No. 1408, 5–8.